https://doi.org/10.15407/ufm.26.01.091

I.E. VOLOKITINA*, A.I. DENISSOVA, and A.V. VOLOKITIN **
Karaganda Industrial University,
30 Republic Ave., 101400 Temirtau, Kazakhstan

* i.volokitina@tttu.edu.kz, irina.vav55@gmail.com, ** a.volokitin@tttu.edu.kz

EVOLUTION OF THE MICROSTRUCTURE OF STEEL IN THE PROCESSES OF SEVERE PLASTIC DEFORMATION

The development of new materials and technologies using various methods of intense energy impacts has brought to the fore the problems of studying the physics of plastic deformation under these conditions. The methods listed in this review include the large or severe plastic deformations, which cause the reduction in grain sizes to the nanoscale level, significant increase in the density of various types defects, deformation phase transformations, and other changes in microstructure, providing new opportunities for modifying not only mechanical, but also fundamental physical properties of materials. In this case, firstly, nonequilibrium structural states including heterophase ones and (or) with a high density of defects and stored deformation energy are formed. Secondly, in these states new mechanisms of plastic flow different from traditional (dislocation) ones appear. Activation of such mechanisms determines the need for their comprehensive study at various from nano- to macrostructural levels, identifying the physical patterns of the formation and evolution of the above-mentioned nonequilibrium structural states, new mechanisms and carriers of plastic deformation.

Keywords: severe plastic deformation, steel, microstructure, structural state, grains.

1. Introduction

Today, there is intensive research development in the field of 'nanotechnology' in many industries. In metallurgical production, this is a reaction to a condition close to exhaustion of the possibilities of creating the required properties of alloys by traditional methods. Grain minimisation is the way to the possible abolition of all metal-forming processes in general. Reducing the size of the particles that make up an object gives it new properties in general. This is caused by, firstly, the influence of developed

Citation: I.E. Volokitina, A.I. Denissova, and A.V. Volokitin, Evolution of the Microstructure of Steel in the Processes of Severe Plastic Deformation, *Progress in Physics of Metals*, **26**, No. 1: 89–119 (2025)

borders, since the border conditions differ from intragrain ones; and secondly, the absence of conditions inside the grain, which manifest themselves in a large volume. Therefore, nanoscale grains can impart substantially new qualities to the same alloy with the same chemical composition. At present, the actual subtle mechanism of this influence has not yet been studied. However, some manifestations in the form of individual abnormally high properties are detected.

The production of metallic nanomaterials in the form of blanks with a volume sufficient for the production of products can be carried out in three ways: by compacting powders with nanoscale particles, intensive plastic deformation and special casting methods. The most attractive way to obtain bulk nanocrystalline materials is severe plastic deformation (SPD), which consists in repeated deformation of the processed materials under conditions close to simple shear [1–10]. The main methods, by which large deformations are achieved, leading to noticeable grain crushing without destroying the sample, are surface smoothing with a solid 5 indenter, high-pressure torsion, equal-channel angular pressing, all-round forging, 'screw' pressing, *etc*. On the one hand, the above-mentioned methods of intensive plastic deformation make it possible, along with reducing the average grain size, to obtain massive samples with an almost porous structure, which cannot be achieved by compacting highly dispersed powders. On the other hand, their main disadvantage is low productivity, which hinders the industrial production of products with the advantages of the properties inherent in the nanostructure. Therefore, in recent years, highly efficient methods for obtaining materials based on rolling and pressing processes have become widely used.

For a long time, one of the postulates in the practice and theory of polycrystalline metallurgy was the statement that it was impossible to grind grains by plastic deformation methods. It was believed that in the process of plastic deformation of polycrystalline grains while maintaining volume with high accuracy, they experience only a shape change (and isomorphically with a change in the shape of the macroform) and change the crystallographic orientation. At the same time, the grains do not lose their identity [11–15]. In other words, until relatively recently it was considered impossible to create large-angle boundaries (bugs) of deformation origin inside the grains. This statement was supported by numerous experimental data, as well as by the basic principles of mechanics and classical dislocation physics of the plasticity of crystalline solids.

Improving the quality of the macro- and microstructure, and therefore the physical and mechanical properties of metal products and semifinished products is one of the urgent tasks of metallurgy and mechanical engineering. To solve such problems, innovative methods, devices and technologies for obtaining materials with a given structure and properties have been created and continue to be created [16–21].

2. Structure and Mechanical Properties of Steels Processed by Equal Channel Angular Pressing

The study of the structure and mechanical properties of steels processed by equal-channel angular pressing (ECAP) is also an urgent problem in materials science. Low plastic properties and high probability of brittle fracture during pressing make it difficult to carry out ECAP of steels; the proportion of edge destroyed volume of material with cracks and 'ridges' and unusable defective workpieces increases. To implement successfully ECAP, a number of technological techniques are usually used to reduce the likelihood of defects, such as increasing of pressing temperature, using backpressure, rounding the angle between the channels, optimizing pressure and pressing speed.

Grain refinement was confirmed during warm ECAP of low-carbon steels Ст3, 20ГСФ and 25Г2С, in which a mixed structure is formed, consisting of SMC grains and subgrains with an average size of 0.35 μm, with an increased density of free dislocations [22]. Carrying out ECAP of low-carbon steels at 500–550 °C allows for four cycles of deformation without destruction of the sample at an angle of intersection of channels $\Phi = 90°$.

Because of the formation of a partially SMC structure, strong strengthening occurs. The yield strength of Ст3 steel was of 840 MPa, which is 3 times higher than in the hot-rolled state, with an elongation of 10.0%. Steels 20ГСФ and 25Г2С are strengthened during warm ECAP to $\sigma_{0.2} = 1110$ and 1000 MPa, respectively, elongation is of 8–11%. Hot ECAP of 20ГСФ steel at 750 °C promotes the formation of a predominantly polygonised structure with fairly high mechanical properties: $\sigma_{0.2} = 905$ MPa, $\delta = 13\%$, $KCV^{+20} = 2$ MJ/m^2.

Chinese scientists [23] studied the effect of ECAP temperature on the structure and mechanical properties of austenitic steel 304L after annealing at 1150 °C for 2 hours and one ECAP pass at 500, 600, 700, 800, and 900 °C, $\Phi = 90°$, $\Psi = 30°$ (Fig. 1). At temperatures below 700 °C, the samples have a lamellar structure with bundles of deformation twins. This microstructure is characterized by high tensile strength but low elongation to break. With increasing processing temperature, return processes occur; more equiaxed subgrains with a low dislocation density, separate bands of twins were formed. The best combination of high strength and ductility was achieved in the sample after ECAP at 800 °C.

Application of deformation by cold ECAP at 20 °C [22] for processing ultra-low carbon automotive sheet steel IF-steel (from interstitial-free, that is, with a small number of interstitial elements) gave a structure that can be characterized as mixed: cellular-subgrain and SMC. IF steel after ECAP has the following properties: relative elongation $\delta = 35\%$, yield strength increases by 3.5 times. It was found that during ECAP at 20 °C austenitic corrosion-resistant steel Х18Н10Т undergoes grinding and ori-

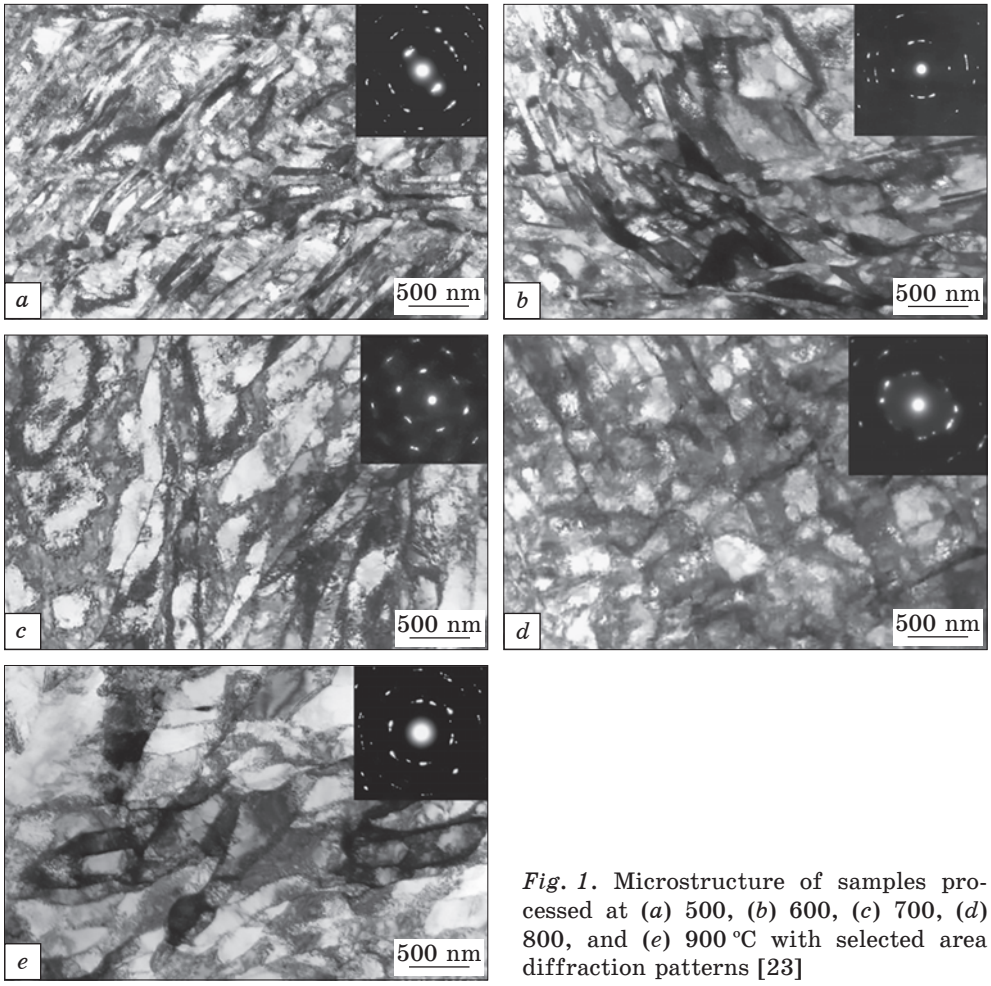

Fig. 1. Microstructure of samples processed at (*a*) 500, (*b*) 600, (*c*) 700, (*d*) 800, and (*e*) 900 °C with selected area diffraction patterns [23]

entation of the structure with a distance between grain boundaries of 100–250 nm. This structure determines significant strain hardening σ_B = 1350 MPa compared to the initial state σ_B = 250 MPa [22].

In Ref. [24], they continued the study of 10Г2ФТ steel, investigating the microstructure and mechanical properties of steel in the initial ferrite-pearlite and martensitic states and after ECAP treatment. Steel with a ferrite-pearlite structure was processed by ECAP at 200 °C (Fig. 2), martensitic steel was processed by ECAP at 400 °C, 4 passes, route B_c, and channel intersection angle was Φ = 120°. After ECAP, an SMC structure with an average fragment size of 0.3 μm was obtained. ECAP of ferrite-pearlite steel led to an increase in strength properties (microhardness and yield strength were doubled). ECAP of martensitic steel causes less pronounced hardening, but the properties after megaplastic deformation ex-

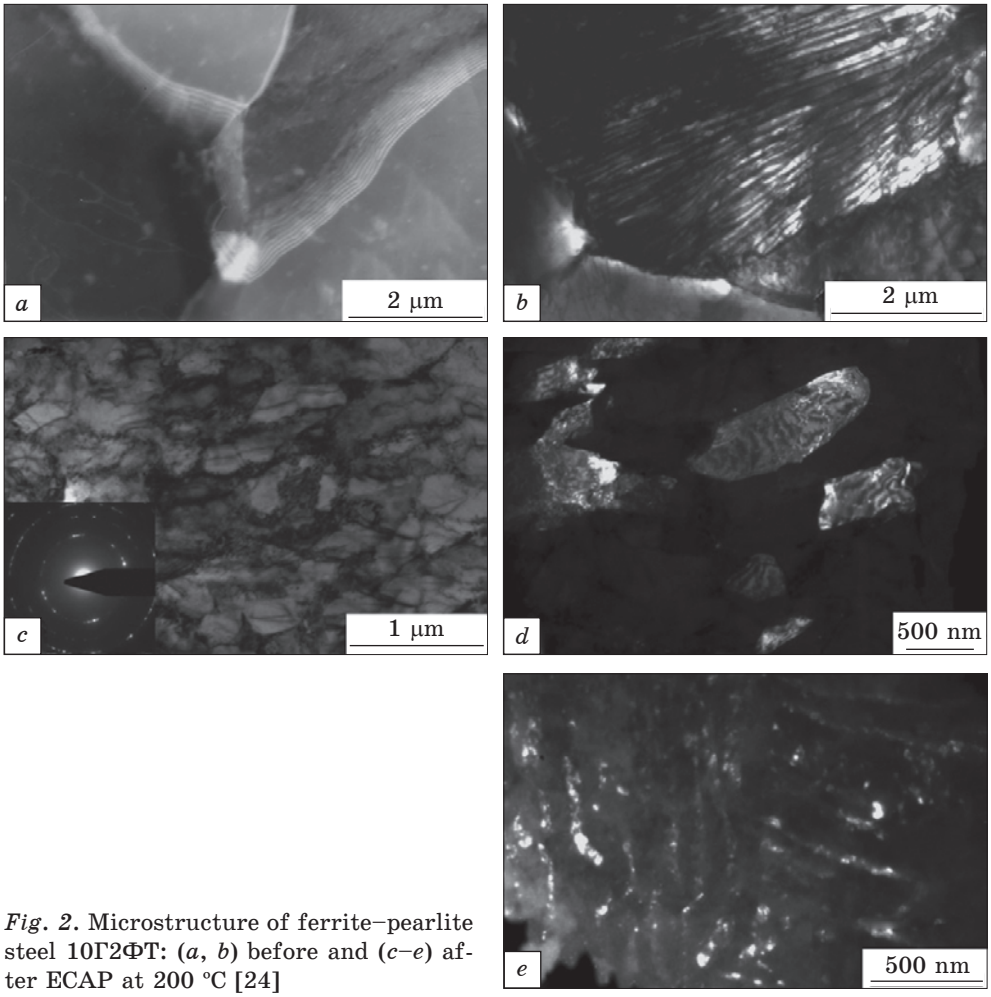

Fig. 2. Microstructure of ferrite–pearlite steel 10Г2ФТ: (*a*, *b*) before and (*c*–*e*) after ECAP at 200 °C [24]

ceed the corresponding properties of ferrite–pearlite steel. Despite the similar sizes of structural elements after ECAP, there is a noticeable difference in the strength characteristics of ferrite-pearlite and martensitic steel. The increase in the mechanical properties of steel after ECAP is due to several factors, such as the formation of an SMC structure, strengthening and the formation of a stress field due to nonequilibrium of boundaries and dislocations.

Article [25] describes the structure and mechanical properties of austenitic steel 08Х18Н10Т after cold ECAP with four deformation cycles (with the 1st cycle, $\Phi = 90°$, and with subsequent cycles, $\Phi = 120°$). After ECAP, a partially submicrocrystalline-oriented structure was obtained with a distance between grain boundaries of 100–250 nm, which provides high strain hardening ($\sigma_{0.2} = 1315$ N/mm^2 *vs.* $\sigma_{0.2} = 250$ N/mm^2 in the ini-

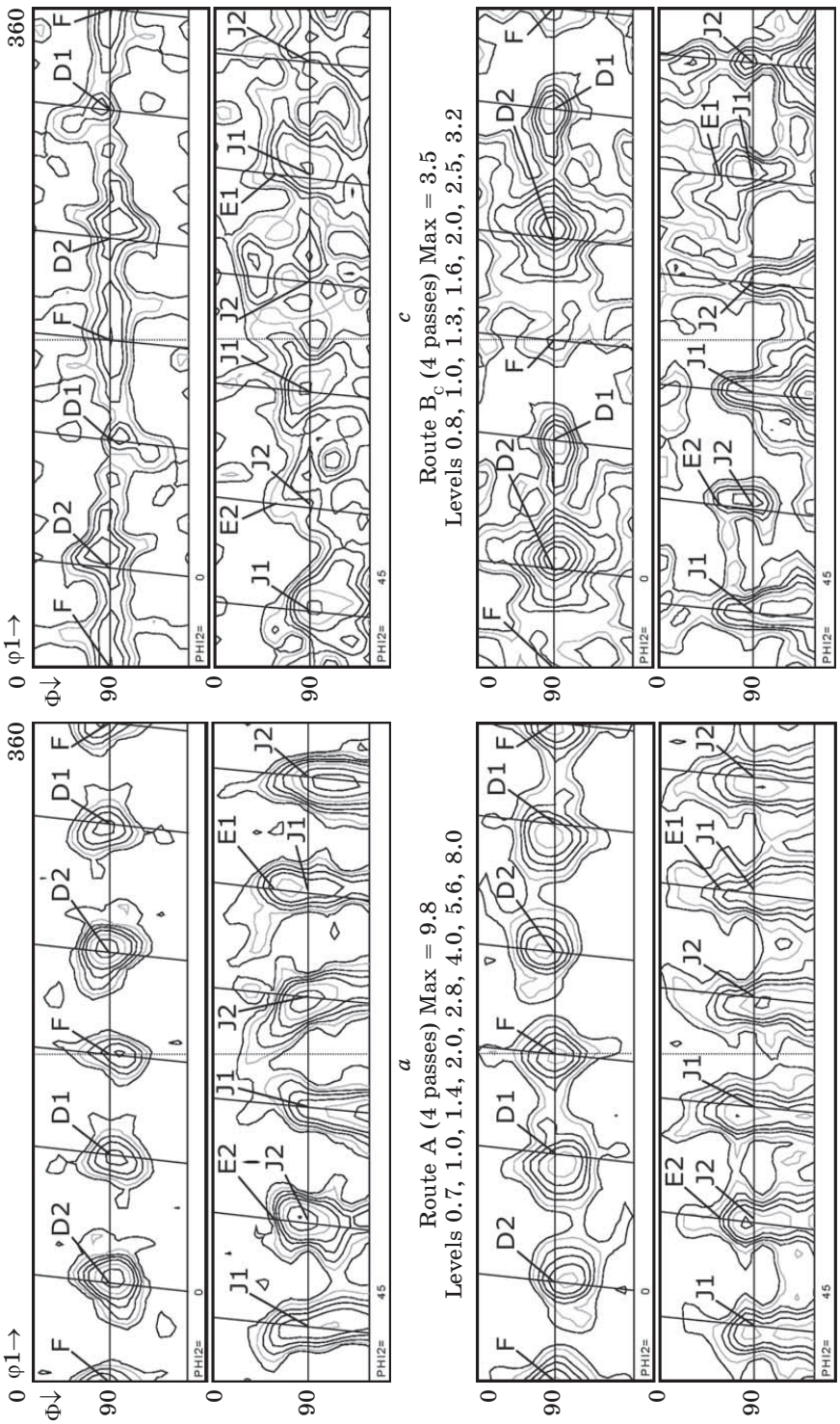

a
Route A (4 passes) Max = 9.8
Levels 0.7, 1.0, 1.4, 2.0, 2.8, 4.0, 5.6, 8.0

b
Route C (4 passes) Max = 3.5
Levels 0.8, 1.0, 1.3, 1.6, 2.0, 2.5, 3.2

c
Route B_C (4 passes) Max = 3.5
Levels 0.8, 1.0, 1.3, 1.6, 2.0, 2.5, 3.2

d
Route B_A (4 passes) Max = 6.7
Levels 0.8, 1.0, 1.3, 1.6, 2.0, 2.5, 3.2, 4.0, 5.0, 6.4

Fig. 3. Sections of the orientation distribution function after 4 ECAP passes along (*a*) route *A*, (*b*) route *C*, (*c*) route B_C and (*d*) route B_A [26]

tial state), and relatively high ductility (δ = 11%). During ECAP at room temperature, austenitic steel 08X18H10T undergoes a martensitic transformation. At N = 4 (ε = 3.2), the martensite content reaches 45%. When heated, martensite (ferrite) transforms into austenite. The transformation occurs most intensively in the temperature range 500–600 °C. After annealing at 550 °C of the ECAP-treated steel, submicrocrystalline austenitic 80.0% and ferritic 20.0% structures were obtained, the yield strength $\sigma_{0.2}$ = 1090 N/mm^2 at plasticity δ = 11.0%.

Belgian scientists [26] studied texturing in IF steel during ECAP with 4 and 8 deformation cycles along various pressing routes A, B_a, B_c, and C (Fig. 3). The microstructure obtained after routes A and C is different, although in both cases reverse deformation occurs between each pass. In routes B_a and B_c, there are significant deviations from monoclinic symmetry, which complicates predicting the further evolution of the structure even after the 2nd pass.

Shagalina *et al*. studied SMC steel 10 and 08P after ECAP with channel intersection angles φ = 90° and 120° at a temperature of 20 °C for the initial ferrite–pearlite structure and at 300°C for the initial bainitic structure along the V_s route. The number of deformation cycles at Φ = 90° was N = 2 for both ECAP temperatures, at Φ = 120° and N = 3 for the initial ferrite–pearlite structure and bainite structure. Heating of samples after ECAP was carried out in the temperature range from 400 to 700 °C with holding for 30 minutes and cooling in water. Cold ECAP of steel 10 with an initial ferrite–pearlite structure leads to the formation of a subgrain, mostly cellular structure, characterized by imperfect boundaries and a high density of free dislocations. There are areas with both an oriented structure and relatively equiaxed structural elements, among which there are grains with high-angle grain boundaries. Normalized steel 08P also has a similar structure. The difference is the lower density of free dislocations and greater perfection of the subgrain boundaries; they are thinner, more oriented structures with a smaller size of structural elements, *i.e*., 230 nm *vs*. 285 nm in steel 10. After ECAP of steels with an initial bainitic structure, there is more perfect, less oriented and more dispersed structure compared to the initial normalized state. There are a significantly larger number of grains with high-angle boundaries; the average grain size was 190 and 245 nm for steel 08P and steel 10, respectively. The smaller grain size after ECAP in steels with an initial bainitic structure can be explained by a higher dislocation density and the presence of dispersed nitrides and carbonitrides. The strength of deformed steel 10 increases by more than 2 times compared to normalized steel 10 (σ_B = = 335 MPa). For steels, the strength and ductility after ECAP are higher with the initial bainitic structure. After heating steels 10 and 08P treated by ECAP to 500 °C, in both cases the orientation of the structure decreases and the size of the structural components increases. Given the general

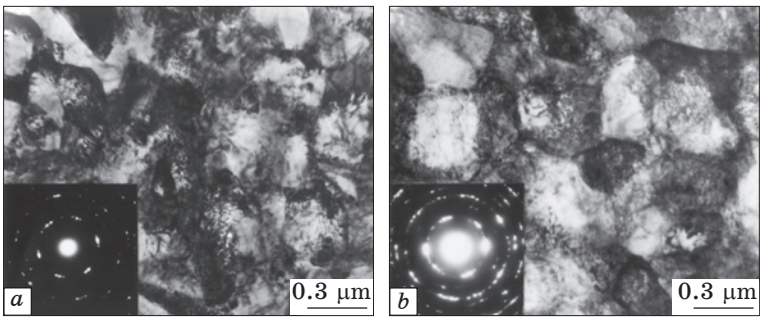

Fig. 4. Ultrafine ferrite grains of steels produced by ECAP at 623 K: (*a*) CS and (*b*) CSV steels [29]

equiaxial nature of the structure after heating, areas with an oriented structure are preserved in all cases. The greatest heterogeneity was observed in steel 10 with an initial ferrite–pearlite structure: the grain size varies within 0.2–5 μm, while individual areas have an oriented subgrain structure [27].

The study [28] compared the ultrafine-grained (UFG) ferrite–pearlite low-carbon steel (Fe–0.15C–0.25Si–1.1Mn), processed by ECAP at 500 °C, 4 pressing cycles, route *C*, and its coarse-grained analogue obtained by heat treatment, annealing at 1200 °C for 1 hour with cooling in air.

Microstructure of ferritic–pearlitic low-carbon steel with chemical composition: 0.15% C, 0.25% Si, 1.1% Mn and 0.15% C, 0.25% Si, 1.1% Mn, 0.06% V after ECAP with four pressing cycles along route *C* is characterized by branched pearlite colonies, UFG ferrite with a grain size of 0.2–0.3 μm, high dislocation density, a large number of low- and high-angle grain boundaries (Fig. 4) [29]. When annealed to 420–500 °C, UFG ferrite grains remain stable with slight grain growth, but microstructural analysis showed that recovery processes are activated, a decrease in dislocation density, restoration of clearly defined grain boundaries and the appearance of a cellular dislocation structure. The strength of UFG ferritic–pearlitic low-carbon steel after ECAP with four pressing cycles along route *C* followed by heating to 730 °C and cooling for 10 minutes is much more than that of the coarse-grained analogue, due to the presence of UFG ferrite and a larger volume fraction of martensite [30–32].

During ECAP, the cementite of pearlite grains dissolves [30–38]. During ECAP and subsequent annealing, dissolved carbon atoms are easily scattered away from pearlite accumulations due to the formation of a high dislocation density and a large number of low- and high-angle grain boundaries after ECAP, *etc*.

The evolution of dislocation processes and the mechanical properties of pure iron treated by ECAP followed by annealing were studied in [39]. An increase in the barriers of dislocation cells is observed after one pass and even more during subsequent pressing cycles. During the ECAP process, after several pressing cycles, low-energy barriers of dislocation cells

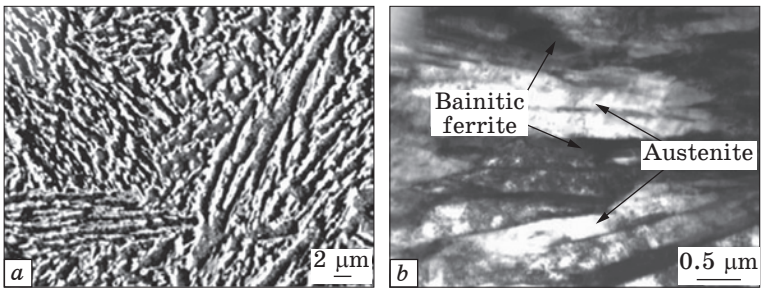

Fig. 5. SEM (*a*) and TEM (*b*) obtained micrographs [41]

transform into a high-energy state, which can lead to softening. Subsequent annealing converts high-energy dislocation structures into low-energy ones, maintaining small grain growth, which allows UFG materials to achieve an excellent combination of high strength and ductility.

In [39], the dynamic characteristics of deformation of UFG low-carbon steel with the following chemical composition were studied: 0.15% C; 0.25% Si; 1.1% Mn after ECAP at 350 °C, $\Phi = 90°$, $\Psi = 20°$, $N = 4$ along route *C*, then, annealing at 480 °C for 1 and 24 hours. The structure of the sample after ECAP consisted of slightly elongated, small grains from 0.2 to 0.3 μm with deformed cementite inside the pearlite grains. During annealing, ferrite grains grew, pearlite dissolved slightly, and fine spherical cementite precipitated at the grain boundaries of ferrite and pearlite regions.

Mechanical tests at room temperature on the original specimens showed that the yield strength, tensile strength and elongation were of 310 and 480 MPa and 30.0%, respectively. After ECAP, the yield strength and strength increased to 937 and 943 MPa, and the elongation decreased to 11.0%. After ECAP and annealing for 1 hour, the values of ultimate strength and yield were of 805 MPa and 823 MPa, elongation of 12.2%; after ECAP and annealing for 24 hours, they were of 713 and 733 MPa, 18.8%, respectively.

A study of the effect of quenching on the structure of low-carbon steel after warm ECAP [40] showed that the resulting structure of UFG ferrite (≈1.3 μm) and localized martensite has greater strength than in hardened steel not treated with ECAP. In Ref. [41], it was revealed that already after the 2nd pass of ECAP, forced (induced) martensite might appear, which was confirmed by TEM (Fig. 5). The high-cycle fatigue properties of most materials increase significantly after SPD and achievement of grain SMC. Grain size reduction and dislocation accumulation play the most important role in the fatigue properties of SMC materials produced by ECAP. Thermal treatment of materials treated with ECAP contributes to a significant improvement in the durability of SMC materials under low-cycle fatigue due to increased ductility and localization of deformation.

Transmission electron microscopy (TEM) of ferritic steel X20 with a tempered martensite structure and a two-component Fe10Cr alloy after

ECAP at 250 °C with one pressing pass, channel intersection angle $\Phi = 90°$, showed the direct interaction of carbides with grain boundaries and their effect on the yield strength [42]. Carbides prevent free dislocations and subgrain boundaries from connecting. It was also found that carbides in contact with grain boundaries coarsen faster than carbides that lost contact during plastic flow.

The authors of Ref. [29] continued their study of UFG of low-carbon steel microalloyed with vanadium. ECAP was carried out at 350 °C, 4 pressing cycles along route *C*, the internal angle of intersection of the channels was 90°, and the arc of rounding was 20°. The UFG structure with ferrite grain sizes of 0.2 and 0.3 μm was obtained in steels with vanadium (initial grain size 10 μm) and without (initial grain size 30 μm), respectively. After annealing of vanadium-free steel above 480 °C, ferrite grains become larger and strength properties deteriorate at room temperature. Vanadium-alloyed steel after annealing up to 540 °C retains high strength properties and submicron grain size. The thermal and mechanical stability of vanadium-containing steel after ECAP is explained by the structural features: blurred pearlite colonies, and ultrafine ferrite grains with evenly distributed nanosize cementite particles. The release of nanosize particles of Fe_3C carbides at the boundaries of ferrite grains in steel containing vanadium occurred due to two main factors: dissolution of carbon from pearlite cementite during SPD, accelerated diffusion of dissolved carbon atoms along the ferrite boundaries and dislocation cores maintaining a high density due to the influence of vanadium on increasing the recrystallization temperature.

Currently, not only the promising properties of materials after ECAP are being studied, but also tests are being carried out on finished products obtained from nanostructured workpieces, which can later be used in industry and medicine.

Using ECAP, authors of Ref. [43] obtained a fastener: an M10 pin, part length of 100 mm, diameter of 10 mm, nominal thread diameter $d = 10$ mm, thread length of nut end at both ends of screw $b = 30$ mm.

The strength class of studs after ECAP at 350°C increased from 4.8 (for studs made of the material in the initial state) to 8.8 after ECAP; in other words, we can talk about obtaining fasteners of a high strength class. The strength of studs after ECAP at 500 °C is 1.7 times greater than that of steel studs in the initial state; the strength class has increased to 6.8.

The literature review showed that ECAP is an effective method for producing SMC and NSMC metals and alloys. Since their intragranular structure, as a rule, contains dislocation substructures with element sizes in the nanorange, metals and alloys processed by ECAP are usually classified as bulk NC materials.

Theoretical works reveal the mechanisms of plastic deformation in the ECAP process and the main patterns of deformation dependence on stress.

In practice, it has been revealed that there is a significant increase in the mechanical characteristics of material. Most works on materials study after ECAP are devoted to the study of changes in the mechanical properties of plastic non-ferrous metals and their alloys [44–46].

3. Structure and Mechanical Properties of Steels Processed by Torsion under High Pressure

Studies carried out on armco iron in Ref. [47] confirm the staged nature of nanostructure formation during severe plastic deformation by torsion. At the first stage, with deformation N from 1/4 to 1 turn, a cellular structure with low-angle misorientations of the boundaries of structural elements and cell sizes of the order of 400 nm. Then, in the second stage, from 1 to 3 revolutions, a transitional structure with signs of a cellular and grain structure is formed. With an increasing degree of deformation, average cell size decreases, and misorientation angles of boundaries are increased, gradually evolving into a homogeneous ultrafine-grained type structure at the third stage. In this case, the grain lattice at the third stage is strongly distorted, because of long-range stresses from nonequilibrium grain boundaries with a high density of grain boundary dislocations. Electron microscopy studies carried out in Ref. [47] after high-pressure torsion (HPT) revealed the similarity of nanostructures formation stages in reinforced iron and in single-phase steels 13X23T and AISI 316L. Almost the only difference is the formation of finer grains in steels at the third stage. Thus, it can be argued that the process of structure formation during HPT of pure metals and alloys has common features. A similar process of nanostructure formation, as well as the dissolution of pearlite plates in industrial pearlitic steel (≈0.7% C) during HPT, was observed in Refs. [48, 49]. After a shear strain of 100 at room temperature, the microstructure of the sample consisted of a cellular structure and partially dissolved cementite plates. A further increase in shear strain to a level of 200 led to a heterogeneous grain structure. During deformation, grains of 100 nm long and 15 nm thick were obtained. Elongated grains were separated by dislocation walls with a high dislocation density. The distance between the cementite plates decreased during deformation. After a shear deformation of 300, uniform nanostructure with a grain size of about 10 nm and complete dissolution of cementite. However, in the XH77TЮP alloy with low stacking fault energy (SFE), a misoriented cellular structure did not form even at very high degrees of deformation. Refinement of the structure occurred with the appearance and propagation of shear bands, which, with increasing deformation, filled the entire volume of the sample. The steady stage of deformation $\varepsilon \geq 5$ is characterized by a structure with regions that practically do not contain dislocations and are misoriented among themselves at large angles. The size of

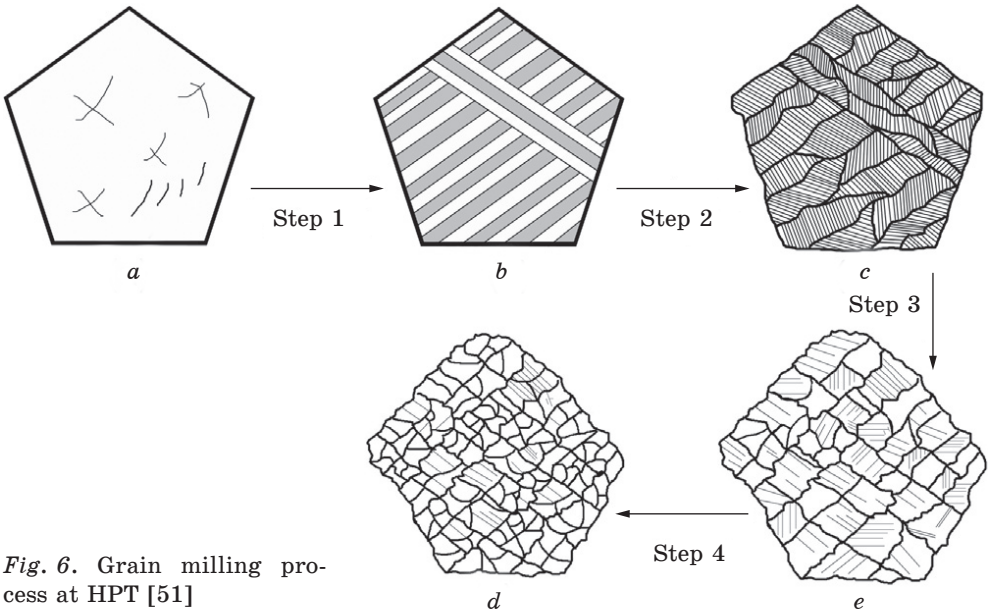

Fig. 6. Grain milling process at HPT [51]

structural elements decreases with decreasing SFE. Work [50] studied the structural changes of ferritic and austenitic steel during torsion under hydrostatic pressure at room temperature. With an equivalent strain equal to $\varepsilon_v = 8$ and 32, the authors obtained a microstructure with an average size of structural elements less than 100 nm. When comparing the results obtained for armco-iron, austenitic and ferritic steel, it was shown that the division of initial grain structure into small crystallites in the case of both steels, compared to armco-iron, is shifted towards lower degrees of deformation. For equivalent strains above $\varepsilon_v = 16$ for steel, no significant changes were observed, and the size of the structural elements is smaller than in armco-iron. The authors of [50] conclude that the decrease in grain size is due to both an increase in the amount of alloying elements and a decrease in the stacking fault energy. Both factors are quite pronounced for steels. Thus, during HPT, the process of structure formation is staged, and the average size of structural elements depends both on the deformation parameters and on the material itself, its SFE and alloying elements.

Different phase components behave differently under the influence of applied strain under the same conditions. Thus, in Ref. [51], duplex stainless steel DP3W with approximately equal volume fractions of ferrite and austenite was studied. During the deformation process, the authors observed two mechanisms of structure formation at once. During HPT, ferrite grain refinement occurred mainly through dislocation activity according to the first mechanism described above. Refinement of austenite structure according to the second mechanism described in Ref. [51] con-

sisted of four stages, as shown in Fig. 6. In the initial state, austenite was a coarse-grained structure with a low density of randomly distributed dislocations (Fig. 6, *a*). At the first stage, during HPT, deformation twins are formed in coarse-grained austenite with an average twin thickness of about 7 nm. In this case, one or two systems of twins in each grain are activated, depending on the orientations of individual grains, which affect the resulting shear stresses in different twinning systems. In the second stage of austenite deformation, a detwinning process occurs, during which stacking faults/secondary nanotwins appear on inclined sliding planes, which, in turn, interact with twins formed at the first stage. The detwinning process increases the distance between twin boundaries from 7 to 200 nm and converts the remaining twin boundaries into conventional high-angle grain boundaries through dislocation–twin boundary interactions, changing the grain size to UFG and significantly increasing the density of secondary twins of ≈1.7 nm. During the deformation process at the third stage, the resulting UFG structure with a large number of twins passes directly through the secondary detwinning, which occurs due to the release of partial dislocations from twin boundaries [52] and grain boundary junctions [53]. The reduced twin density obtained by secondary detwinning engages dislocation activity [54], which leads to active interaction between dislocations and twin boundaries and the subsequent transformation of remaining twin boundaries into ordinary high-angle grain boundaries. The result is grains with an average grain size of ≈30 nm. At the fourth stage of deformation, stacking faults and nanotwins are continuously formed due to the separation of partial dislocations from grain boundaries into nanocrystalline grains. Further deformation occurs through interactions between newly formed dislocations and nanotwins [55], leading to further grain refinement to an average size of ≈23 nm.

Work [50] shows that, compared to ferritic steel and other materials, structural elements in austenitic steel at the same level of severe plastic deformation are much smaller and more uniform in size. With an increase in plastic deformation to the equivalent deformation $\varepsilon_v = 32$, structural elements become refined. Due to more alloying elements and lower stacking fault energy, austenitic steel contains fewer structural elements than ferritic steel and armco iron. In addition, in Ref. [50], austenitic steel samples were heated after HPT at 700, 750, and 800 °C, as well as, for comparison, ferritic steel at 450, 500, and 550 °C with a holding time of 1 hour. The first visible structural changes were noticed at the lowest annealing temperatures. During the study [50], with increasing annealing temperature in ferritic steel, the size of structural elements increased from 100 nm (at 450 °C) to 500 nm (at 550 °C), and in austenitic steel, from 80 nm (at 700 °C) to 350 nm (at 800 °C). The authors of Ref. [50] concluded that the structure after HPT in austenitic steel is thermally more stable than in ferritic steel. The initially high temperatures, at which

the first structural changes appear in austenitic steel and the smaller size of structural elements after annealing, compared to ferritic steel, are a consequence of both the presence of a large number of alloying elements and lower stacking fault energy in austenitic steel.

When studying structure formation in the process of HPT of austenitic stainless steel 12X18H10T in works [105, 106], the formation of a submicrocrystalline structure characterized by a high density of stacking faults, presence of twins, deformation localization bands, and formation of a cellular structure characteristic of materials with high SFE was revealed The authors of [56] proposed the following description of the processes of structure formation during HPT. After compression (≈8 GPa), crushed microstructure is characterized by the presence of microtwins and dislocation cells. Bands of localized deformation indicate uneven deformation. Microdiffraction from a section of such a band is blurred reflections in the form of arcs. During torsion ($\varepsilon \approx 1.8$), a finely dispersed structure appears along with twins and stacking faults. The presence of the ε-phase in the form of ordered twins in the γ-matrix was also noticed. With an increase in the degree of logarithmic deformation (up to $\varepsilon \approx 3.2$), proportion of finely dispersed components with the phase composition $\varepsilon + \gamma + \alpha$ increases, with an average size of structural elements $d \approx 110$ nm. In the diffraction patterns, point reflections are observed from areas with twins, and blurred reflections in the form of arcs from areas of a cellular structure. Next stage ($\varepsilon \approx 3.9$) is characterized by a very heterogeneous structure, with fragments of crushed twins and large fragments of size $d \approx 200$ nm. With an average crystallite size of $d \approx 90$ nm, the average size of structural elements was $d \approx 30$–40 nm. With an increase in the degree of deformation (up to $\varepsilon \approx 5.1$), the structure becomes refined ($d \approx 60$ nm), as a result, due to the many reflections from the structural elements, an almost annular diffraction pattern is observed. Further increase in the degree of deformation ($\varepsilon \approx 5.5$) leads to a finer structure ($d \approx 45$ nm) and, as a consequence, to a more diffuse diffraction pattern. However, there are regions consisting of structural elements with close orientation with a size of about 500 nm.

4. Features and Mechanisms of Plastic Deformation

The development of dislocation–disclination approaches in works led to the construction of model concepts of collective mechanisms of transformation in an ensemble of defects and relaxation of highly defective structural states with crystal lattice curvature, characterized by components of the bending–torsion tensor associated with local internal stresses. In Refs. [57–59], it was proposed to associate these structural states with the implementation of the flexural deformation mode. It is noted that this defor-

mation mechanism operates along with translational (movement of individual dislocations) and collective rotational deformation modes.

Among these patterns, we note the concept of multi-stage and multiscale structural levels of deformation and destruction of solids, hierarchy of these levels, and, accordingly, deformation mechanisms, developed in Ref. [60]. According to this concept, plastic deformation develops simultaneously at several structural levels, while plastic translations at the microlevel are accompanied by rotations of the crystal lattice and localization of deformation at the mesolevel.

Mesodefects, containing both shear and rotational components of deformation, make it possible to move volumetric structural elements of various scales in a deformed solid: subgrains, grains, their conglomerates, extended blocks of material.

Thus, plastic deformation is transmitted to the macro level with subsequent macrolocalization and destruction of the sample. For the first time, ideas about collective dislocation–disclination modes of plastic flow under conditions of large plastic deformations were developed in Ref. [61]. It is shown that, under these conditions, the deformation mechanisms change from uncorrelated dislocation glide to plastic reversals because of collective effects in dislocation ensembles of strongly interacting dislocations at their high density. These mechanisms are realized at the mesolevel of deformation and ensure fragmentation of the initial grains with the formation of misoriented fragments.

In some of the works, ideas were developed according to which in zones of local curvature the concentration of nonequilibrium non-thermal vacancies increases significantly (by several orders of magnitude), bifurcations arise interstitial structural states that change the electronic energy spectrum of the crystal. They determine the development of a fundamentally new effect, *i.e.*, plastic distortion, which plays a leading role in the generation and crystallographic sliding of dislocations and other phenomena of plastic deformation.

Strain-induced phase (martensitic) transformations are important mechanisms of plastic deformation in many metallic materials [62]. In the process of such transformations, stable martensitic phases or stable two-phase (martensite + austenite) states are formed. In this case, during the process of plastic deformation, the formation of metastable martensitic phases is possible, which upon completion of deformation are transformed into stable phases. Classic example is the $\gamma \rightarrow \varepsilon \rightarrow \alpha'$ transformation in austenitic steels, in which stable α'-martensite is formed through a metastable ε-phase [62], traces of which are detected experimentally. In alloys undergoing thermoelastic martensitic transformations, martensitic phases existing under load transform into the original stable phase upon unloading, while the implementation of the reverse transformation according to the same system is a condition for reversibility and restoration of shape [63].

The works [57–59] propose quasi-viscous (diffusion) mechanisms of plastic deformation and reorientation of the crystal lattice by flows of nonequilibrium point defects in fields of high local stresses. It is shown that these mechanisms are important mechanisms of nanostructuring in the process of large plastic deformations of metals with f.c.c. and b.c.c. lattices and mechanisms of plastic deformation in nanostructural states. Concepts have been introduced about new deformation carriers 'nanodipoles of partial disclinations' or non-crystallographic shear dislocations as zones of inhibited elastic shears and rotations. It has been shown that the main factors determining the implementation of non-dislocation (or collective dislocation) deformation mechanisms are the formation of nonequilibrium, high-strength, including nanostructural states with high curvature of the crystal lattice and the impossibility of their relaxation by the sliding of individual dislocations.

In the work of Kolubaev *et al*. [64], the dependence on the scale of deformation of the subsurface layer of a metal material during friction was studied, and the processes of stress localization during sliding friction were considered. As shown, stress localization leads to intense fragmentation in the subsurface layer and the formation of slip bands in the pre-fragmented material. These slip bands are initially at the microscale, but when they reach the stage of catastrophic wear, they can move to the mesoscale level of deformation. The result of this transition is the appearance of a thin nanocrystalline layer on the metal surface. Microstructural changes in the subsurface layer of solids during friction consist in fragmentation of the original structure and subsequent formation of a fragmented (nanocrystalline) layer, which completely changes the type of deformation and wear mechanism during sliding friction. The first stage of sliding is characterized by the formation of a localized deformation zone with a fragmented internal structure. The fragment size is about 20 nm. Nanoscale substructural fragments can form a mesoscale vortex structure under the worn surface. An increase in stress fragments the structure, which determines the formation of wear particles. Deformational incompatibility between the nanocrystalline top layer and the fragmented material promotes the formation of cavities, depressions and cracks that appear at the boundaries of these layers.

The nanocrystalline layer was obtained in medium carbon steel by high-energy shot peening [65]. The tribological characteristics of the nanocrystalline layer were studied during dry sliding using the ring-disk friction scheme. The study of surface topography shows that the nanocrystalline layer can improve the tribological properties of medium carbon steel. Experimental results at low normal load showed that, after obtaining a nanocrystalline layer, the coefficient of friction and mass wear are reduced and, as a result, wear resistance increases. When the load is below 40 N, surface failure occurs because of ploughing and microcutting with abrasive particles removed from the surface of the sample, leaving multiple

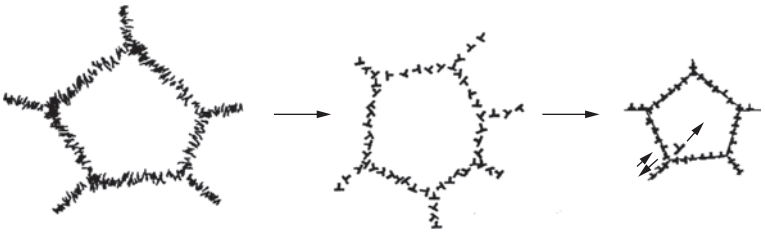

Fig. 7. Scheme of UFG microstructure development according to the model described in Ref. [67]

wear marks on the surface. At a load of 40 N, fatigue cracks appear on the worn surface, but the wear mechanism remains abrasive. When the load exceeded 40 N, large changes were revealed on the friction surface due to plastic displacement of the material and surface fatigue failure of the deformed layer. Changes in the microgeometry of the surface showed that at loads above 50 and 60 N, the wear mechanism was replaced by fatigue.

After friction treatment of pearlitic carbon steel 1080 [66], a martensitic structure of a surface layer 5 mm deep was obtained. Tribological tests on a pin-disc friction machine showed that the treated surface during dry friction has a 25.0% lower friction coefficient compared to the initial state, the wear value has decreased by an order of magnitude due to a decrease in the surface layer plasticity; friction with lubricant is mainly determined by the lubricating medium.

The most well-known models explaining grain refinement during SPD are described in Refs. [67–70]. These models differ only in some areas and in all cases are based on the assumption that the reduction in grain size is associated with the accumulation and growth of dislocations. This situation is shown schematically in Fig. 7.

Large deformations lead to an increase in dislocation density, with preference given to concentration in cells. It is known that oppositely directed dislocations cancel each other out, so new low-angle grain boundaries are formed first by polygonization. This is a continuous process, in which the maximum grain refinement that can be achieved is limited by reduction processes and saturation occurs at very high elongation. However, there is a dependence on the material itself, in particular on the number of phases, the energy of stacking defects and temperature [71–75]. On the one hand, it is known, there is a maximum dislocation density, which can be achieved. Thus, the grain size is limited, since grain refinement in the presented model directly depends on the change in the dislocation structure [76]. Accordingly, with increasing massive plastic deformation, only grain rotation occurs at higher misorientation angles, but not a decrease in grain size [71, 77]. On the other hand, the phenomenon of grain boundary migration, which leads to the minimum grain size achieved under massive plastic deformation, is considered decisive [67, 78].

Unlike Valiev's model [67], the Hughes and Hansen model [68] also explains the development of a preferred direction in microstructure. This

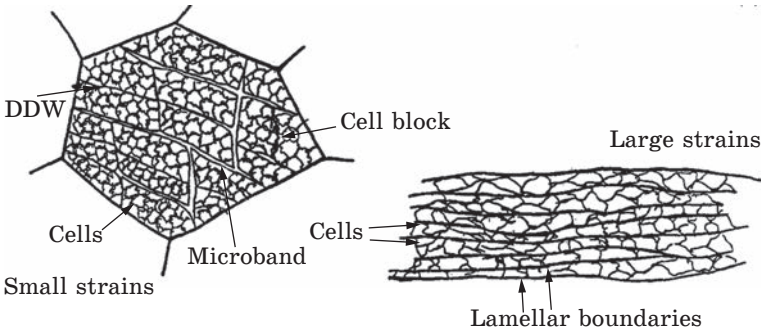

Fig. 8. Scheme of UFG microstructure development following the model described in Ref. [68]

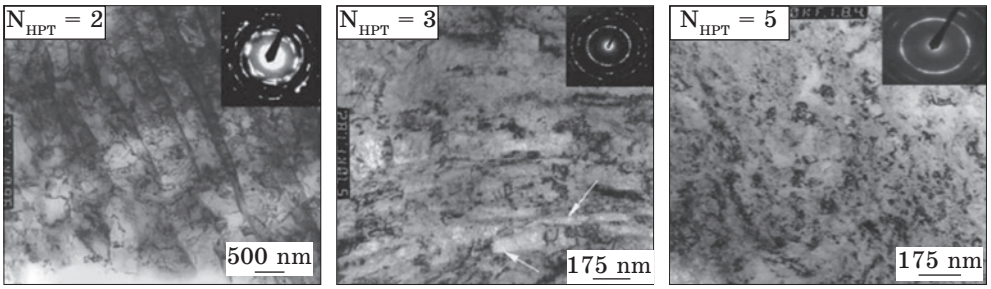

Fig. 9. TEM images of the microstructure of UIC 860 steel after different number of rotations [49]

requires a division into random dislocation boundaries (IDBs) and geometrically necessary boundaries (GNBs). In Figure 8 shows different types of substructures in the refined microstructure.

IDBs correspond to polygonal dense dislocation walls and form the smallest unit. They can be combined with neighbouring cells into blocks of cells. In the case of small deformations, blocks of cells are separated from each other by microstrips or dense dislocation walls, which are part of the geometrically necessary boundaries.

When transitioning to large deformations, preference is given to lamellar boundaries, the so-called shear bands, which order dislocation cells [68, 69]. Geometrically necessary subgrain boundaries typically exhibit misorientation in the high angle range above 15° much more rapidly than random dislocation boundaries. They experience an increase in disorientation.

Figure 9 shows the change in the microstructure of ferrite-pearlite steel at different stages of severe plastic deformation.

At the first stage, studies [49] showed the formation of a lamellar cellular structure with a predominance of low-angle grain boundaries. After three revolutions, individual nanostructured regions gradually appear

with still elongated grains, the diameter of which is about 100 nm. As shown by the arrows, the grains are partially separated by dense dislocation cell walls, which is consistent with the theory of Hughes and Hansen [68, 69]. Partially continuous and more pronounced Debye–Scherrer rings indicate the development of new high-angle grain boundaries. After further deformation of five revolutions, a polycrystalline and homogeneous nanostructure with an average grain size of 10 nm was formed. This is also indicated by the sharply defined and continuous Debye–Scherrer rings, on which, however, after ten revolutions, the cementite spots are no longer visible. Consequently, cementite dissolved, which was also demonstrated in Ref. [79] using alternative measurement methods. These results are consistent with other literature data [79–85], mainly related to massive plastic deformation at room temperature.

At elevated temperatures, only nanostructured cementite particles at grain boundaries were detected in Ref. [86], but complete dissolution of cementite was not observed.

Temperature plays an important role in SPD, especially when using hard and high-strength materials. When produced at room temperature, cracks or other irregularities often occur. In addition, the materials usually become very brittle after processing and are not thermally stable [48]. There are basically two heat treatment options to improve these properties. Firstly, SPD is carried out directly at elevated temperatures (usually, 350–400 °C for steels), which also has a positive effect on the formability and strengthening ability of the deformed material [86–89]. On the other hand, heat treatment can also be carried out after massive plastic deformation. This provides a reduction in dislocation accumulation and can reduce the strong thermodynamic imbalance at grain boundaries and thereby improving the mechanical properties, in particular the ductility of the material [87, 90]. However, especially in aluminium alloys, precipitation processes can also affect the mechanical properties during heat treatment after SPD [91]. In contrast to the widespread explanation of grain refinement by polygonization of dislocations and the resulting formation of a substructure, alternative explanations are also found in the literature. For example, [92] and [93] suggest that continuous dynamic recrystallization occurs based on dynamic reduction, which can result in the formation of very fine dislocation-free grains.

5. Peculiarities of Deformation Localization in the Stable Austenitic Steels

In most metallic materials, including austenitic steels, at large degrees of deformation, and a transition occurs from uniform deformation to localization of deformation at various scale levels. In this case, areas of intense plastic flow appear in the material, which at the micro level repre-

sent localized shear bands or localized deformation bands (LDB). This section focuses on shear-type deformation localization bands, as the most characteristic defect structures of austenitic steels, formed under conditions of large plastic deformations. Significant shear deformation is localized in these bands, and a wide range of crystal lattice misorientations and nanostructural states are formed.

There are two types of bands. The first type develops in a lamella structure consisting of twin/matrix (T/M) layers lamella) [94, 95]. Bands of this type are characteristic of many f.c.c. metals with low (≤20 mJ/m^2) and medium (20–40 mJ/m^2) SFE, as well as for materials with high (40 mJ/m^2 or more) SFE under specific conditions of low temperatures and high strain rates.

The second type of PLD develops in a microstrip structure consisting of dislocation formations with low-angle boundaries, namely, double dense dislocation walls and low-energy dislocation substructures [96]. These bands are formed in many materials with high SFE under deformation conditions at room temperature [96, 97], in austenitic steels under deformation conditions at high temperatures [98, 99] and in steels of other classes: ferritic, martensitic, *etc*. [100].

To date, the features of the microstructure and mechanisms of formation of first-type PLDs in copper and copper alloys under conditions of dynamic plastic deformation at cryogenic temperatures have been studied in most detail. The formation conditions and microstructure features of these strips are in many ways similar to those in austenitic steels.

The formation of localization bands is a characteristic feature of austenitic steels' deformation structure after medium (*i.e.*, true deformation $\varepsilon \approx 0.7–1.2$) degrees of deformation [101]. It has been established that their main feature is the presence of significant shear deformation. Shear bands are plate-like regions of material, within which shears are concentrated, parallel to the plane of occurrence of the band. These stripes cross grain boundaries without changing the orientation of this plane.

Therefore, the geometry of their distribution is determined more by the geometry of the deformation process than by the crystallography of deformed material [101]. During rolling, shear bands are formed in the form of plates inclined by 20–55° (most often ≈35°) to the rolling direc-tion [101].

During the process of shear-bands' formation features that arise during cold rolling of 316L stainless steel [101], it was shown that these bands are formed in the range of deformation degrees of 70–90% in grains that are characterized by layered structures consisting of twin lamellas approximately parallel to the plane rolling. After deformation $\varepsilon \approx 70\%$, these stripes consist of plates (≈1 μm long and 0.1 μm wide) elongated in the shear direction. At a degree of deformation of 90%, they are divided into equiaxial cells of ≈10 nm in size. In the longitudinal section of the sample, rhombuses with an internally twinned structure are observed,

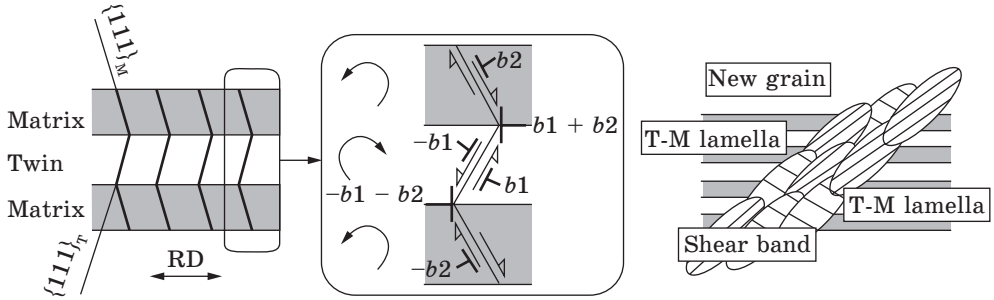

Fig. 10. Process of deformation localization band generation: *a* — diagram of the lamella structure, *b* — sliding and rotations in layers, *c* — formation of new PLD grains (shear band) [102]

formed by shear bands of two systems; the nucleation of a shear band on strongly curved deformation twins was also observed [101].

It was shown in Ref. [102] that, when a PLD passes through layered structures consisting of T/M lamellas, the crystal lattice in the twin rotates clockwise, and in the matrix counterclockwise. This behaviour is explained [102] using the model presented in Fig. 10. With an increase in the degree of deformation during rolling, the T/M lamellas become almost parallel to the rolling plane (Fig. 10, *a*), which leads to increased sliding in the {111} planes intersecting the boundaries lamellas, both in the matrix and twin regions. Sliding in these planes causes the crystal to rotate clockwise in the twin region, and counterclockwise in the matrix region (Fig. 10, *b*). As a result, the orientation of each layer changes, deviating from the original orientation of the twin and matrix. In addition, the activation of slip leads to the accumulation of a high dislocation density near twin boundaries. Local annihilation of dislocations of different signs occurs with the formation of new boundaries (Fig. 10, *c*). The annihilation of these boundaries enhances additional sliding, during which the emergence of new boundaries continues. The width of the deformation localization band increases with increasing degree of deformation; the T/M lamella structure is destroyed with the formation of a fine-grained (nanocrystalline) structure (Fig. 10, *b*) [102].

Increasing the degree of sample deformation leads to an increase in the degree of localized deformation inside the PLD. The shear band expands; within the band, fragmentation of the crystal lattice intensively develops with the formation of misoriented nanosize fragments.

During the formation of UFG structures, the dislocation density increases significantly, and accordingly, dislocation strengthening also undergoes significant changes. When the dislocation density in the metal exceeds 10^6–10^8 cm^{-2}, their elastic interaction with each other begins to affect itself, causing inhibition of gliding dislocations and, as a conse-

quence, an increase in shear stresses. The main process of mobile-dislocations' braking is considered to be their intersection with 'scaffold' dislocations, *i.e.*, with dislocations that do not lie in the primary slip plane of the moving dislocation. As a result, dislocation clusters are formed, creating elastic stress fields that gradually block the sources of dislocations.

Potential barriers caused by the interaction of dislocations can be divided into long-range and short-range.

Long-range stresses are caused by the elastic stress fields of dislocations and their groups. Short-range stresses are associated with short-range order forces acting at a distance of several lattice periods and arising when dislocations intersect, split, and form thresholds, kinks, and dislocation dipoles.

Taylor (see monography [103] and references therein) suggested that the inhibition of an individual dislocation is due to its elastic long-range interaction with dislocations forming a periodic structure in the crystal. Seeger subsequently took into account the influence of groups of primary dislocations at the second stage of hardening, creating long-range stress fields [103]. However, Seeger's theory [103] does not take into account the formation of cellular structures and entanglements of dislocations, characteristic of the real dislocation structure of deformed metals.

The Kuhlmann–Wilsdorf theory [103] explains strain hardening by fields of short-range stresses caused by the forces of deflection of gliding dislocations between 'scaffold' dislocations and the formation of loops around them. The model takes into account the possibility of cellular dislocation structure formation during deformation.

Adjacent to the theory of hardening by short-range stress fields are theories that connect strain hardening with the inhibition of screw or mixed dislocations with the formation of thresholds on them because of mutual intersection. According to Gilman's theory [103], when dislocations move with thresholds, dislocation dipoles are formed, *i.e.*, stable pairs of closely spaced dislocations of the opposite sign, chains of vacancies and interstitial atoms, which impede the movement of other dislocations.

Long-term studies of the fragmentation phenomenon have led to the conclusion that in polycrystals its root cause is powerful elastic stresses, the sources of which arise at grain boundaries and joints. Essentially, fragmentation is the result of plastic accommodation, heterogeneity of which in the grain volume manifests itself in the form of fragmented substructure. It is near the junctions or morphological features of original boundaries (steps, ledges, and bends) that the emergence of new boundaries is observed, which grow inside the grains and divide them into crystalline elements misoriented among themselves. As for the driving force of this process, *i.e.*, internal stresses, then their sources (plastic incompatibilities) accumulate at the boundaries due to differences in the intrinsic plastic deformations of adjacent grains. The appearance of such incompatibilities is inevitable because crystal grains are differently oriented rela-

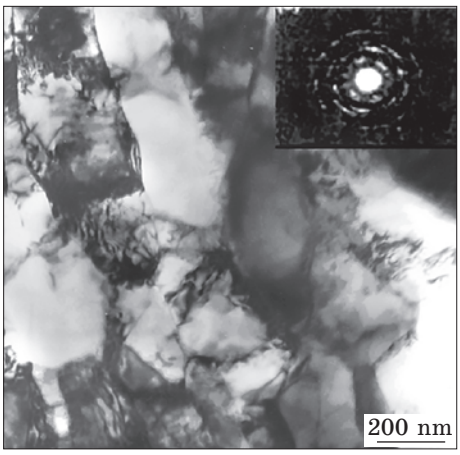

Fig. 11. Fragmented substructure of low- and medium-carbon steel after SPD [106]

tive to macroscopic deforming stresses and therefore exhibit different plastic compliance. However, as misorientations between emerging fragments grow, the process described above is reproduced at their boundaries and junctions, forming a new generation of fragments, *etc*. The homogeneous orientation of the lattice inside the structural elements turns out to be unstable concerning plastic deformation, and the fragmentation process is continuous. An important role in the process of crystal lattice fragmentation during the formation of a submicrocrystalline structure is played by the dislocation–disclination mechanism of crystal lattice reorientation, including the formation of the above-mentioned substructures with a high excess density of dislocations of the same sign and their subsequent rearrangements into localized misorientation boundaries [104].

Thus, a fragmented substructure is a substructure of mutually misoriented regions (subgrains) separated by low-angle and medium-angle dislocation subboundaries (fragment walls). A fragmented substructure is formed both because of heat treatment and during the deformation of steel [105]. In Ref. [106], attempts were made to study the fragmented substructures of low and medium-carbon steels. As seen in Fig. 11, the dislocation cells with a high dislocation density are observed in equiaxed ferrite grains. This leads to the manifestation of fundamentally new physical and mechanical properties in them.

Plastic deformation, as a rule, proceeds inhomogeneously [104, 107]. The heterogeneity of plastic deformation can manifest itself on different scales and for various reasons. During technological processes, under conditions of complex deformation, various types of dislocation substructures are formed in a metal material. In this case, it is necessary to take into account that during plastic deformation the defect substructure also evolves [107, 109], various defects and their complex formations appear and disappear in the volume of the deformed material, remaining defects change structure parameters, and therefore knowledge of nature and patterns of defective substructure evolution is necessary. The authors of Ref. [104], studying defect evolution of substructure during large plastic deformations of the alloy by torsion on Bridgman anvils, believe that an important feature of the defect substructure at the first stage of deformation, as in the case of rolling deformation, is the high density of submi-

crocrystals with high continuous misorientations or high boundary density with variable misorientation vectors, modelled by clusters of continuously distributed partial disclinations of the same sign. This type of substructure has now been discovered in a wide class of submicrocrystalline materials: Cu, Ni, *etc*. The sources of inhomogeneous stresses leading to the formation of substructures with high curvature of the crystal lattice can be either dislocation ensembles with a high excess density of dislocations of the same sign, or a continuous accumulation distributed partial disclinations within boundaries with variable misorientation vectors [104, 108].

Transmission electron microscopy methods were used to study the defect substructure and phase composition of metastable austenitic steel after large plastic deformations by rolling [58]. Because of martensitic transformations, regions with a predominant content of one of the phases and two-phase ($\gamma + \alpha'$) regions are observed. As the degree of deformation increases, a two-phase fragmented substructure with fragment sizes of submicrocrystalline and nanocrystalline scales is formed in steel. Fragments with high-angle misorientations are also recognized. It has been shown that characteristic features of the defect structure of austenite are the formation of deformation micro- and nanotwins, and localization bands with an internal fragmented structure. A dislocation substructure is formed inside submicron- and nanocrystals, with a dislocation density of up to 10^{12} cm^{-2}. In addition, the formation of nanosize plates of deformation martensite was discovered inside individual fragments. When studying the substructure and internal stresses of the same type of austenitic steel by other authors [107] during hot deformation, it was found that the change in microstructure is characterized by the evolution of subgrains with dense dislocation boundaries. These subgrains become more equiaxed and misoriented, and the stress between them gradually increases, eventually leading to the formation of fine grains with an average size of about 0.3 μm. The evolution of such new thin grain formation can be facilitated by any rearrangement of dislocations at their boundaries. In addition, some new fine grains evolve at high stresses and contain dislocations within them, resulting in a decrease in the average dislocation density as fine grains develop. On the other hand, these fine grains are characterized by high curvature of the crystal lattice.

Thus, the problem of dislocation accumulation in deformed materials remains complex and largely unsolved. This statement applies to both pure metals and solid solutions with relatively simple dislocation substructures, and to materials with a complex substructure. In these materials, phase transformations can occur before or during plastic deformation. A typical example is the substructures formed in martensitic steels, in which, along with grains, there are dislocation cells, fragments, packets and plates. Similar structures, when some boundaries are located inside other substructural formations, can arise during plastic deformation in ultrafine-

grained polycrystals [110], especially under conditions of dynamic recrystallization and other processes. In the size range corresponding to micrograins and microfragments, other patterns in the accumulation of dislocations appear in comparison with the patterns in the mesoregion. This phenomenon is characteristic of both ultrafine-grained polycrystals and small fragments observed in deformed martensitic steels. The authors of Ref. [111] experimentally established empirical dependences of the scalar dislocation density on the size of fragments and cells in deformed martensitic steel. They found that the type of dislocation structure in steel fragments decisively determines the dependence of the scalar dislocation density on their size. If there is a network dislocation substructure inside the fragments, then, the scalar dislocation density decreases with decreasing fragment size. On the contrary, if the dislocation substructure in fragments is cellular, then with decreasing fragment size the scalar dislocation density increases. As the cell size decreases, the dislocation density also increases rapidly. This behaviour is due to different mechanisms of braking of gliding dislocations in the network and cellular dislocation substructures. The relationships between various parameters of dislocation substructure established in the work are fundamental for the further development of metals and alloys dislocation strengthening physics. The dislocation paradigm of substructural hardening receives in such relationships, firstly, direct confirmation and, secondly, reveals the fundamental role of substructural formations in the dislocation concept of hardening physics.

6. Conclusions

The analytical review showed that currently, despite a large number of scientific studies, there is no data on structural changes under complex loading conditions and their influence on the formation of mechanical properties. The predominant number of studies was carried out under standardized testing conditions using compression, tension, and torsion, as well as technological tests with a constant mechanical deformation scheme.

Until now, a large amount of work has been done on the development of deformation methods using SPD and the study of fundamental and applied properties for various metals and alloys. It has been established that for most metal alloys, the evolution of the microstructure under the influence of SPD is associated with phase transformations occurring in them. In other words, the structural–phase state of alloys after severe deformation may be different from what it was before deformation.

Acknowledgement. This research is funded by the Science Committee of the Ministry of Science and Higher Education of the Republic of Kazakhstan (Grant No. AP19678974).

REFERENCES

1. P. Kolesnikov, *Prog. Phys. Met.*, 24, No. 1: 132 (2023); https://doi.org/10.15407/ufm.24.01.132
2. I. Volokitina, N. Vasilyeva, R. Fediuk, and A. Kolesnikov, *Materials*, **15**: 3975 (2022); https://doi.org/10.3390/ma15113975
3. I.E. Volokitina, A.V. Volokitin, and E.A. Panin, *Prog. Phys. Met.*, **23**, No. 4: 684–728 (2022); https://doi.org/10.15407/ufm.23.04.684
4. I.E. Volokitina and A.V. Volokitin, *Metallurgist*, **67**: 232 (2023); https://doi.org/10.1007/s11015-023-01510-7
5. I. Volokitina, B. Sapargaliyeva, A. Agabekova, A. Volokitin, S. Syrlybekkyzy, A. Kolesnikov, G. Ulyeva, A. Yerzhanov, and P. Kozlov, *Case Studies Construct. Mater.*, **18**: e02162 (2023); https://doi.org/10.1016/j.cscm.2023.e02162
6. A.V. Volokitin, I.E. Volokitina, E.A. Panin, *Prog. Phys. Met.*, **23**, No. 3: 411 (2022); https://doi.org/10.15407/ufm.23.03.411
7. I. Volokitina, A. Volokitin, A. Denissova, T. Fedorova, D. Lawrinuk, A. Kolesnikov, A. Yerzhanov, Y. Kuatbay, and Y. Liseitsev, *Case Studies Construct. Mater.*, **19**: e02346 (2023); https://doi.org/10.1016/j.cscm.2023.e02346
8. I. Volokitina, A. Volokitin, E. Panin, T. Fedorova, D. Lawrinuk, A. Kolesnikov, A. Yerzhanov, Z. Gelmanova, and Y. Liseitsev, *Case Studies Construct. Mater.*, **19**: e02609 (2023); https://doi.org/10.1016/j.cscm.2023.e02609
9. I. Volokitina, A. Bychkov A. Volokitin, and A. Kolesnikov, *Metallogr. Microst. Anal.*, **12**, No. 3: 564–566 (2023); https://doi.org/10.1007/s13632-023-00966-y
10. N. Zhangabay, I. Baidilla, A. Tagybayev, U. Suleimenov, Z. Kurganbekov, M. Kambarov, A. Kolesnikov, G. Ibraimbayeva, K. Abshenov, I. Volokitina, B. Nsanbayev, Y. Anarbayev, and P. Kozlov, *Case Studies Construct. Mater.*, **18**: e02161 (2023); https://doi.org/10.1016/j.cscm.2023.e02161
11. I.E. Volokitina, *Metal Sci. Heat Treat.*, **61**: 234 (2019); https://doi.org/10.1007/s11041-019-00406-1
12. I. Volokitina, A. Volokitin, and D. Kuis, *J. Chem. Technol. Metallurgy.*, **56**: 643 (2021); https://journal.uctm.edu/node/j2021-3/25_20-126p643-647.pdf
13. I.E. Volokitina, *Metal Sci. Heat Treat.*, **62**: 253 (2020); https://doi.org/10.1007/s11041-020-00544-x
14. I.E. Volokitina, *Prog. Phys. Met.*, **3**: No. 24: 593 (2023); https://doi.org/10.15407/ufm.24.03.593
15. S. Lezhnev, A. Naizabekov, E. Panin, and I. Volokitina, *Procedia Engineering*, **81**: 1499 (2014); https://doi.org/10.1016/j.proeng.2014.10.180
16. S. Lezhnev A. Naizabekov, A. Volokitin, and I. Volokitina, *Procedia Engineering*, **81**: 1505 (2014); https://doi.org/10.1016/j.proeng.2014.10.181
17. S. Lezhnev, A. Naizabekov, and I. Volokitina, *J. Chem. Technol. Metallurgy.*, **52**, No. 4: 626 (2017); https://journal.uctm.edu/node/j2017-4/3_17-04_Lezhnev_p_626-635.pdf

18. S. Lezhnev, I. Volokitina, and T. Koinov, *J. Chem. Technol. Metallurgy.*, **49**, No. 6: 621 (2014);
https://journal.uctm.edu/node/j2014-6/14-Koinov-621-630.pdf
19. A. Volokitin, I. Volokitina, and E. Panin, *Metallogr. Microst. Anal.*, **11**, No. 4: 673 (2022);
https://doi.org/10.1007/s13632-022-00877-4
20. S. Lezhnev, E. Panin, and I. Volokitina, *Adv. Mater. Res.*, **814**: 68 (2013);
https://doi.org/10.4028/www.scientific.net/AMR.814.68
21. S.V. Dobatkin, A.M. Arsenkin, M.A. Popov, and A.N. Kishchenko, *Metal Sci. Heat Treat.*, **47**: 188 (2005);
https://doi.org/10.1007/s11041-005-0050-2
22. C.X. Huang, G. Yang, Y.L. Gao, S.D. Wu, and Z.F. Zhang, *Mater. Sci. Eng. A*, **485**: 643 (2008);
https://doi.org/10.1016/j.msea.2007.08.067
23. E.G. Astafurova, G.G. Zakharova, E.V. Naydenkin, S.V. Dobatkin, and G.I. Raab, *Phys. Metals Metallogr.*, **110**: 260 (2010);
https://doi.org/10.1134/S0031918X10090097
24. S.V. Dobatkin, O.V. Rybalchenko, and G.I. Raab, *Russ. Metallurgy*, **1**: 42 (2006).
25. J. De Messemaeker, B. Verlinden, and J. Van Humbeeck, *Acta Mater.*, **53**: 4245 (2005);
https://doi.org/10.1016/j.actamat.2005.05.024
26. S.V. Shagalina, E.G. Koroleva, G.I. Raab, M.V. Bobylev, and S.V. Dobatkin, *Russ. Metallurgy*, **3**: 219 (2008).
27. Y.I. Son, Y.K. Lee, and K.T. Park, *Metall. Mater. Trans. A*, **37**: 3161 (2006);
https://doi.org/10.1007/s11661-006-0196-6
28. K.-T. Park, Y.-S. Kim, and D.H. Shin, *Metall. Mater. Trans. A*, **32**: 2373 (2001);
https://doi.org/10.1007/s11661-001-0211-x
29. D.H. Shin, B.C. Kim, Y.S. Kim, K.-T. Park, *Acta Mater.*, **48**: 2247 (2000);
https://doi.org/10.1016/S1359-6454(00)00028-8
30. D.H. Shin, B.C. Kim, K.-T. Park, and W.Y. Choo, *Acta Mater.*, **48**: 3245 (2000);
https://doi.org/10.1016/S1359-6454(00)00090-2
31. D.H. Shin, Y.S. Kim, and E.J. Lavernia, *Acta Mater.*, **49**: 2387 (2001);
https://doi.org/10.1016/S1359-6454(01)00165-3
32. K.-T. Park and D.H. Shin, *Mater. Sci. Eng.*, **334**: 79 (2002);
https://doi.org/10.1016/S0921-5093(01)01796-8
33. D.H. Shin, K.-T. Park, and Y.S. Kim, *Scripta Mater.*, **48**: 469 (2003);
https://doi.org/10.1016/S1359-6462(02)00512-2
34. I.E. Volokitina, *Metal Sci. Heat Treat.*, **63**: 163 (2021);
https://doi.org/10.1007/s11041-021-00664-y
35. A.B. Naizabekov, S.N. Lezhnev, and I.E. Volokitina, *Metal Sci. Heat Treat.*, **57**, Nos. 5–6: 254 (2015);
https://doi.org/10.1007/s11041-015-9870-x
36. A.B. Nayzabekov and I.E. Volokitina, *Phys. Metals. Metallogr.*, **120**, No. 2: 177–183 (2019);
https://doi.org/10.1134/S0031918X19020133
37. I.E. Volokitina and A.V. Volokitin, *Phys. Metals Metallogr.*, **119**, No. 9: 917–921 (2018);
https://doi.org/10.1134/S0031918X18090132
38. B.Q. Han, E.J. Lavernia, and F.A. Mohamed, *Metall. Mater. Trans. A*, **35**: 1343 (2004);
https://doi.org/10.1007/s11661-004-0309-z

39. K.-T. Park, S.Y. Han, B.D. Ahn, D.H. Shin, Y.K. Lee, and K.K. Um, *Scripta Mater.*, **51**: 909 (2004); https://doi.org/10.1016/j.scriptamat.2004.06.017
40. F. Hajiakbari, M. Nili-Ahmadabadi, B. Poorganji, and T. Furuhara, *Acta Mater.*, **58**: 3073 (2010); https://doi.org/10.1016/j.actamat.2010.01.044
41. A. Kostka, K.-G. Tak, R.J. Hellmig, Y. Estrin, and G. Eggeler, *Acta Mater.*, **55**: 539–550 (2007); https://doi.org/10.1016/j.actamat.2006.08.046
42. P.G. Mordovskoi, M.Z. Borisova, S.P. Yakovleva, S.N. Maharova, *IV Int. Conf. Functional Nanomaterials and High-Purity Substances (2012)*, p. 25.
43. I. Volokitina, A. Volokitin, B. Makhmutov, *Symmetry*, **16**, No. 8: 997 (2024); https://doi.org/10.3390/sym16080997
44. A. Naizabekov, A. Arbuz, S. Lezhnev, E. Panin, and I. Volokitina, *Physica Scripta*, **94**, No. 10: 105702 (2019); https://doi.org/10.1088/1402-4896/ab1e6e
45. I.E. Volokitina and G.G. Kurapov, *Metal Sci. Heat Treat.*, 59, Nos. 11–12: 786 (2018); https://doi.org/10.1007/s11041-018-0227-0
46. R.Z. Valiev, Yu.V. Ivanisenko, E.F. Rauch, and B. Baudelet, *Acta Mater.*, **44**: 4705 (1997).
47. Y. Ivanisenko, R.K. Wunderlich, R.Z. Valiev, and H.J. Fecht, *Scripta Mater.*, 49: 947 (2003).
48. Y. Ivanisenko, W. Lojkowski, R.Z. Valiev, and H.J. Fecht, *Acta Mater.*, **51**: 5555 (2003).
49. A. Vorhauer, S. Kleber, and R. Pippan, *Ultrafine Grained Materials III* (TMS: 2004), p. 629.
50. Y. Cao, Y.B. Wang, X.H. An, X.Z. Liao, M. Kawasaki, S.P. Ringer, T.G. Langdon, and Y.T. Zhu, *Acta Mater.*, **63**: 16–29 (2014); https://doi.org/10.1016/j.actamat.2013.09.030
51. J. Wang, N. Li, O. Anderoglu, X. Zhang, A. Misra, J.Y. Huang, and J.P. Hirth, *Acta Mater.*, **58**: 2262 (2010); https://doi.org/10.1016/j.actamat.2009.12.013
52. Y. Wei, *Mater. Sci. Eng. A*, **528**: 1558 (2011); https://doi.org/10.1016/j.msea.2010.10.072
53. Y. Cao, Y.B. Wang, Z.B. Chen, X.Z. Liao, M. Kawasaki, S.P. Ringer, T.G. Langdon, and Y.T. Zhu, *Mater. Sci. Eng. A*, **578**: 110 (2013); https://doi.org/10.1016/j.msea.2013.04.075
54. S. Ni, Y.B. Wang, X.Z. Liao, R.B. Figueiredo, H.Q. Li, S.P. Ringer, T.G. Langdon, and Y.T. Zhu, *Acta Mater.*, **60**: 3181 (2012); https://doi.org/10.1016/j.actamat.2012.02.026
55. B. Efros, V. Pilyugin, A. Patselov, S. Gladkovskii, N. Efros, L. Loladze, and V. Varyukhin, *Mater. Sci. Eng. A*, **503**: 114 (2009); https://doi.org/10.1016/j.msea.2008.01.096
56. S.V. Bobylev and I.A. Ovid'ko, *Acta Mater.*, **124**: 333 (2017); https://doi.org/10.1016/j.actamat.2016.11.026
57. Y. Li, B. Gu, S. Jiang, Y. Liu, Z. Shi, and J. Lin, *Int. J. Plasticity*, **134**: 102844 (2020); https://doi.org/10.1016/j.ijplas.2020.102844
58. C. Xu. M. Furukawa, Z. Horita, and T.G. Langdon, *Nanostructured Materials by High-Pressure Severe Plastic Deformation* (Eds. Y.T. Zhu and V. Varyukhin) (Dordrecht: Springer: 2006), p. 201;

https://doi.org/10.1007/1-4020-3923-9_28
59. M.P. Kashchenko, V.V. Letuchev, L.A. Teplyakova, and T.N. Yablonskaya, *Fiz. Met. Metalloved.*, **82**, No. 4: 10 (1996) (in Russian).
60. A.D. Korotaev, A.N. Tyumentsev, and Y.P. Pinzhin, *Theoretical and Applied Fracture Mechanics*, **35**: 163 (2001).
61. S.J. Wang, *Nature Communications*, 5: 3433 (2014).
62. *Shape Memory Materials* (Eds. K. Otsuka and C.M. Wayman) (Cambridge University Press: 1998).
63. A. Kolubaev, S. Tarasov, O. Sizova, and E. Kolubaev, *Tribology Int.*, **43**: 695 (2010); https://doi.org/10.1016/j.triboint.2009.10.009
64. G. Li, J. Chen, and D. Guan, *Tribology Int.*, 43: 2216 (2010); https://doi.org/10.1016/j.triboint.2010.07.004
65. S.H. Aldajah, O.O. Ajayi, G.R. Fenske, and S. David, *Wear*, **267**: 350 (2009); https://doi.org/10.1016/j.wear.2008.12.020
66. R.Z. Valiev, Y.V. Ivanisenko, E.F. Rauch, and B. Baudelet, *Acta Mater.,* **44**: 4705 (1996); https://doi.org/10.1016/S1359-6454(96)00156-5
67. D.A. Hughes and N. Hansen, *Acta Mater.*, **45**: 3871 (1997); https://doi.org/10.1016/S1359-6454(97)00027-X
68. R.D. Doherty, *Mater. Sci. Eng. A*, **238**, No. 2: 219 (1997); https://doi.org/10.1016/S0921-5093(97)00424-3
69. M.A. Meyers, *Mater. Sci. Eng. A*, **317**: 204 (2001); https://doi.org/10.1016/S0921-5093(01)01160-1
70. R. Pippan, F. Wetscher, M. Hafok, A. Vorhauer, and I. Sabirov, *Advanced Eng. Mater.*, **8**: 1046 (2006); https://doi.org/10.1002/adem.200600133
71. I.E. Volokitina and A.V. Volokitin, *Phys. Metals Metallogr.*, **119**, No. 9: 917 (2018); https://doi.org/10.1134/S0031918X18090132
72. G. Kurapov, E. Orlova, I. Volokitina, and A. Turdaliev, *J. Chem. Technol. Metall.*, **51**, No. 4: 451 (2016); https://journal.uctm.edu/node/j2016-4/13-Volokitina_451-457.pdf
73. I. Volokitina, *J. Chem. Technol. Metall.*, **57**, No. 3: 631 (2022); https://journal.uctm.edu/node/j2022-3/24_21-123_br_3_pp_631-636.pdf
74. V. Chigirinsky and I. Volokitina, *Engineering Solid Mechanics*, **12**, No. 2: 113 (2024); https://doi.org/10.5267/j.esm.2023.11.001
75. J. Gubicza, N.Q. Chinh, Gy. Krallics, I. Schiller, and T. Ungar, *Current Appl. Phys.*, **6**: 194 (2006); https://doi.org/10.1016/j.cap.2005.07.039
76. H.J. Maiera, P. Gabor, N. Gupta, I. Karaman, and M. Haouaoui, *Internat. J. Fatigue*, **28**: 243 (2006); https://doi.org/10.1016/j.ijfatigue.2005.05.004
77. R. Pippan, S. Scheriau, A. Taylor, M. Hafok, A. Hohenwarter, and A. Bachmaier, *Annual Rev. Mater. Res.*, **40**: 319 (2010); https://doi.org/10.1146/annurev-matsci-070909-104445
78. S.N. Lezhnev, I.E. Volokitina, and A.V. Volokitin, *Phys. Metals Metallogr.*, **118**, No. 11: 1167 (2017); https://doi.org/10.1134/S0031918X17110072
79. I. Volokitina, B. Sapargaliyeva, A. Agabekova, S. Syrlybekkyzy, A. Volokitin, L. Nurshakhanova, F. Nurbaeva, A. Kolesnikov, G. Sabyrbayeva, A. Izbassar, O. Kolesnikova, Y. Liseitsev, and S. Vavrenyuk, *Case Studies Construct. Mater.*, **19**: e02256 (2023); https://doi.org/10.1016/j.cscm.2023.e02256

80. A. Volokitin, I. Volokitina, and E. Panin, *J. Mat. Res. Technol.*, **31**: 2985 (2024); https://doi.org/10.1016/j.jmrt.2024.07.038
81. I.E. Volokitina, A.I. Denissova, A.V. Volokitin, and E.A. Panin, *Prog. Phys. Met.*, **25**, No. 1: 132 (2024); https://doi.org/10.15407/ufm.25.01.132
82. I.E. Volokitina, A.I. Denissova, A.V. Volokitin, T.D. Fedorova, and D.N. Lavrinyuk, *Prog. Phys. Met.*, **25**, No. 1: 161 (2024); https://doi.org/10.15407/ufm.25.01.161
83. I. Volokitina, N. Vasilyeva, R. Fediuk, and A. Kolesnikov, *Materials*, **15**, No. 11: 3975 (2022); https://doi.org/10.3390/ma15113975
84. A. Volokitin A. Naizabekov I. Volokitina, and A. Kolesnikov, *J. Chem. Technol. Metallurgy.*, **57**, No. 4: 809 (2022); https://journal.uctm.edu/node/j2022-4/20_22-18_br4_2022_pp809-815.pdf
85. J. Ning, E. Courtois-Manara, L. Kurmanaeva, A.V. Ganeev, R.Z. Valiev, C. Kübel, and Y. Ivanisenko, *Mater. Sci. Eng. A*, **581**: 8 (2013); https://doi.org/10.1016/j.msea.2013.05.008
86. A. Nurumgaliyev, T. Zhuniskaliyev, V. Shevko, Y. Mukhambetgaliyev, B. Kelamanov, Y. Kuatbay, A. Badikova, G. Yerekeyeva, and I. Volokitina, *Sci. Rep.*, **14**, No. 1: 7456 (2024); https://doi.org/10.1038/s41598-024-57529-6
87. L.W. Meyer, M. Hockauf, B. Zillmann, and I. Schneider, *Int. J. Mater. Form.*, **2**: 61 (2009); https://doi.org/10.1007/s12289-009-0545-2
88. P.R. Cetlin, M.T.P. Aguilar, R.B. Figueiredo, and G. Langdon, *J. Mater. Sci.*, **45**: 4561 (2010); https://doi.org/10.1007/s10853-010-4384-9
89. A. Hohenwarter, C. Kammerhofer, and R. Pippan, *J. Mater. Sci.*, **45**: 4805 (2010); https://doi.org/10.1007/s10853-010-4635-9
90. K. Hockauf, L.W. Meyer, M. Hockauf, and T. Halle, *J. Mater. Sci.*, **45**: 4754 (2010); https://doi.org/10.1007/s10853-010-4544-y
91. J.-Q. Su, T.W. Nelson, and C.J. Sterling, *Scripta Mater.*, **52**: 135 (2005); https://doi.org/10.1016/j.scriptamat.2004.09.014
92. T. Belyakov, H. Sakai, K. Miura, and A. Ts, *Philos. Mag. A*, **81**, No. 11: 2629 (2001); https://doi.org/10.1080/0141861011004287
93. H. Miyamoto, A. Vinogradov, S. Hashimoto, and R. Yoda, *Mater. Trans.*, **50**: 1924 (2009); https://doi.org/10.2320/matertrans.M2009054
94. L. Bracke, K. Verbeken, L. Kestens, and J. Penning, *Acta Mater.*, **57**, No. 2: 1512 (2009).
95. D.A. Hughes and N. Hansen, *Acta Mater.*, **48**: 2985 (2000); https://doi.org/10.1016/s1359-6454(00)00082-3
96. Y.B. Wang, X.Z. Liao, Y.H. Zhao, E.J. Lavernia, S.P. Ringer, Z. Horita, T. Langdon, and Y.T. Zhu, *Mater. Sci. Eng. A*, **527**, Nos. 18–19: 4959 (2010); https://doi.org/10.1016/j.msea.2010.04.036
97. P. Cizek, F. Bai, M. Rainforth, and J.H. Beynon, **45**: 2157 (2004); https://doi.org/10.2320/matertrans.45.2157
98. M.C. Mataya, M.J. Carr, and G. Krauss, *Metall. Trans. A*, **15**: 347 (1994); https://doi.org/10.1007/BF02645121
99. B. Hwang, S. Lee, Y.C. Kim, N.J. Kim, and D.H. Shin, *Mater. Sci. Eng. A*, **441**: 308 (2006);

https://doi.org/10.1016/j.msea.2006.08.045
100. C. Donadille, R. Valle, P. Dervin, and R. Penelle, *Acta Metall.*, **37**, No. 6: 1547 (1989);
https://doi.org/10.1016/0001-6160(89)90123-5
101. T. Morikawa and K. Higashida, *Proc. of the 21st RISO Int. Symp. on Materials Science* (Denmark: RISO National Laboratory: 2000), p. 476.
102. Ulrich Messerschmidt, *Dislocation Dynamics during Plastic Deformation* (Berlin–Heidelberg: Springer: 2010);
https://doi.org/10.1007/978-3-642-03177-9
103. I.A. Ditenberg, A.N. Tyumentsev, K.V. Grinyaev, V.M. Chernov, M.M. Potapenko, and A.V. Korznikov, *Tech. Phys.*, **56**: 815 (2011);
https://doi.org/10.1134/S106378421106003X
104. G. Krauss, *Metall. Mater. Trans. B*, **32**: 205 (2001);
https://doi.org/10.1007/s11663-001-0044-4
105. S. Dobatkin, J. Zrnik, and I. Mamuzic, *Metallurgija*, **47**, No. 3: 181 (2008).
106. A. Belyakov, T. Sakai, H. Miura, and R. Kaibyshev, *Scripta Mater.*, 42: 319 (2000);
https://doi.org/10.1016/S1359-6462(99)00353-X
107. Y. Son, Y. Lee, K. Park, Ch. Lee, and D. Shin, *Acta Mater.*, **53**: 3125 (2005);
https://doi.org/10.1016/j.actamat.2005.02.015
108. H. Zheng, H. Ye, J. Li, L. Jiang, Z. Liu, C. Wang, and B. Wang, *Mater. Sci. Eng. A*, **527**: 7407 (2010);
https://doi.org/10.1016/J.MSEA.2010.08.023
109. M. Calcagnotto, Y. Adachi, D. Ponge, and D. Raabe, *Acta Mater.*, **59**: 658 (2011);
https://doi.org/10.1016/j.actamat.2010.10.002
110. J. Moon, S.-J. Kim, and Ch. Lee, *Mater. Sci. Eng. A*, **28**: 7658 (2011);
https://doi.org/10.1016/j.msea.2011.06.067

Received 12.06.2024
Final version 01.02.2025

І.Є. Волокітіна, А.І. Деніссова, А.В. Волокітін
Карагандинський індустріальний університет,
просп. Республіки, 30, 101400 Темиртау, Казахстан

ЕВОЛЮЦІЯ МІКРОСТРУКТУРИ СТАЛІ В ПРОЦЕСАХ ІНТЕНСИВНОЇ ПЛАСТИЧНОЇ ДЕФОРМАЦІЇ

Розроблення нових матеріалів і технологій із застосуванням різних методів інтенсивних енергетичних впливів поставило на перший план завдання вивчення фізики пластичної деформації в цих умовах. Наведені в цьому огляді методи включають великі або інтенсивні пластичні деформації, що спричинюють зменшення розмірів зерен до наномасштабного рівня, значне збільшення щільності дефектів різного типу, деформаційні фазові перетворення та інші зміни мікроструктури, які забезпечують нові можливості модифікування не тільки механічних, але й фундаментальних фізичних властивостей матеріалів. Водночас, по-перше, формуються нерівноважні структурні стани, зокрема гетерофазні та (або) з високою щільністю дефектів і запасеною енергією деформації. По-друге, у цих станах виявляються нові, відмінні від традиційних (дислокаційних) механізми пластичної течії. Активізація таких механізмів визначає необхідність їх комплексного дослідження на різних від нано- до макроструктурних рівнях, виявлення фізичних закономірностей формування й еволюції зазначених вище нерівноважних структурних станів, нових механізмів і носіїв пластичної деформації.

Ключові слова: інтенсивна пластична деформація, сталь, мікроструктура, структурний стан, зерна.